

Maximizing Spectral Flux from Self-Seeding Hard X-ray FELs

Xi Yang*

Brookhaven National Laboratory, Upton, NY 11973, USA

Yuri Shvyd'ko†

Advanced Photon Source, Argonne National Laboratory, Argonne, Illinois 60439, USA

(Dated: March 26, 2022)

Fully coherent x-rays can be generated by self-seeding x-ray free-electron lasers (XFELs). Self-seeding by a forward Bragg diffraction (FBD) monochromator has been recently proposed [1] and demonstrated [2]. Characteristic time \mathcal{T}_0 of FBD determines the power, spectral, and time characteristics of the FBD seed [3]. Here we show that for a given electron bunch with duration σ_e the spectral flux of the self-seeding XFEL can be maximized, and the spectral bandwidth can be respectively minimized by choosing $\mathcal{T}_0 \sim \sigma_e/\pi$ and by optimizing the electron bunch delay τ_e . The choices of \mathcal{T}_0 and τ_e are not unique. In all cases, the maximum value of the spectral flux and the minimum bandwidth are primarily determined by σ_e . Two-color seeding takes place if $\mathcal{T}_0 \ll \sigma_e/\pi$. The studies are performed, for a Gaussian electron bunch distribution with the parameters, close to those used in the short-bunch ($\sigma_e \simeq 5$ fs) and long-bunch ($\sigma_e \simeq 20$ fs) operation modes of the LCLS XFEL.

PACS numbers: 41.50.+h, 41.60.Cr, 61.05.cp, 42.55.Vc

I. INTRODUCTION

Seeded x-ray free-electron lasers (XFELs) [2, 4] generate fully coherent x-rays with a well-defined spectrum and higher spectral flux. Their supreme spectral properties will expand the science reach of the XFELs, and stimulate the utilization of advanced high-resolution spectroscopic techniques. The self-seeding XFEL is also a path to increase the peak radiation power of XFELs to the TW levels [5]. In the present paper we study the conditions for stable seeding, with the smallest shot-to-shot variations of output radiation, the narrowest bandwidth, and largest spectral flux.

The self-seeding scheme uses x-rays from the first half of the FEL system (electron beam – magnetic undulator system – radiation field) to generate radiation by the self-amplified spontaneous emission (SASE) process [6–10] to seed the electron bunch in the second half of the FEL system via an x-ray monochromator [11, 12]. The delay of x-rays in the monochromator is compensated by the appropriate delay τ_e of the electron bunch in the magnetic chicane. Standard x-ray monochromators produce delays in the picosecond range, at least. In the hard x-ray regime with high-energy electrons, a large magnetic chicane is required to match the path-length delay of the x-ray monochromator, which may degrade the electron-beam qualities. A possible solution is using a two-electron-bunch self-seeding scheme [13]. Another elegant solution, proposed by Geloni, Kocharyan,

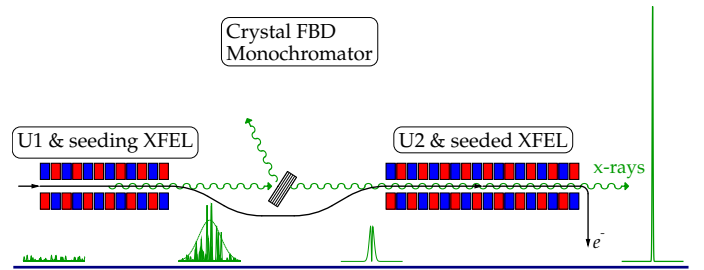


FIG. 1: (Color online) Hard x-ray FEL self-seeding scheme uses x-rays from the first half of the magnetic undulator system U1 to seed the electron bunch in the second half U2 via a single crystal x-ray monochromator. The monochromator produces the delayed monochromatic seed under the forward Bragg diffraction (FBD) conditions [1].

and Saldin, uses forward Bragg diffraction (FBD) of x-rays from a diamond crystal to generate a monochromatic seed [1] - Fig. 1. The first trailing maximum of FBD was proposed for the self-seeding of $\simeq 5$ -fs (FWHM) short electron bunches, at an optimal ≈ 20 -fs delay of the seed relative to the electron bunch. The proposal have been recently realized and fully coherent hard x-rays have been generated at the LCLS XFEL by an international team led by Emma [2].

The question that naturally arises is: Under what conditions is seeding most efficient in terms of achieving the shortest XFEL saturation length, the smallest spectral bandwidth of output radiation, and the largest spectral density? One could expect that for this, generally speaking, the monochromatic seed duration should be comparable to the duration of the electron pulse, the monochromatic seed power should substantially exceed the shot

*Electronic address: xiyang@bnl.gov

†Electronic address: shvydko@aps.anl.gov

noise power, and the peak seed power should overlap with the peak electron current density. The question then concretizes to which crystal, which Bragg reflection, which scattering geometry, which crystal thickness, etc. suit best? This is a problem with many parameters, which is difficult to tackle. However, there is a possibility to reduce the problem to one single parameter.

It has been shown in [3] that under a certain approximation the time dependence of FBD can be characterized by a single parameter \mathcal{T}_0 , the time constant of forward Bragg diffraction. It is the main parameter that defines the strength, and duration of the FBD monochromatic seed. It is a generic feature for all symmetric or asymmetric, for all transmission (Laue-case) or reflection (Bragg-case) scattering geometries. The physics is controlled by the parameters that compose \mathcal{T}_0 : the magnitude of the effective crystal thickness (crystal thickness seen by the incident beam), and the extinction length in the symmetric Bragg reflection (characteristic length of Bragg diffraction). This approximation is correct if we are interested in the FBD radiation emanating from the crystal with delays t , which are significantly shorter than a mere propagation time \mathcal{T}_d of the radiation through the crystal. It turns out that exactly for self-seeding applications the approximation $t \ll \mathcal{T}_d$ holds well in many cases.

Due to this property, the spectral flux optimization could be studied by analyzing self-seeding as a function of the principle time constant \mathcal{T}_0 . With one more time constant \mathcal{T}_d taken into account, a more accurate picture can be achieved. Here we perform such studies using the 3D time-dependent FEL simulation code GENESIS 1.3 by Sven Reiche [14].

The paper is organized as follows. In Sec. II we briefly summarize the basic properties of Bragg diffraction (BD) and the complementary to it forward Bragg diffraction (FBD), and outline the procedure to calculate the monochromatic seed in forward Bragg diffraction from a crystal in the XFEL self-seeding scheme. In Sec. III we provide details on the 3D FEL simulations. In Sec. IV we present and discuss the results of the simulations.

II. GENERATION OF THE MONOCHROMATIC SEED IN FBD

A. Basic Properties of Forward Bragg Diffraction

Here we briefly summarize the basic properties of Bragg diffraction (FB) and of the complementary forward Bragg diffraction (FBD); define their characteristic spectral, time, and space parameters; and outline, using results and notations of [3], the procedure for calculating the monochromatic seed in FBD from a crystal in the XFEL self-seeding scheme.

Bragg diffraction (BD) of x-rays incident upon a crystal at a glancing angle θ to reflecting atomic planes with diffraction vector \mathbf{H} , see Fig. 2 (left), takes place within a spectral range ΔE_H centered at a photon energy $E_c = Hc\hbar/2\sin\theta$, defined by Bragg's law. Here c is the speed of light in vacuum, and \hbar is Planck's constant. An example Bragg reflection spectral dependence $|R_{0H}(E)|^2$ is shown in Fig. 2(a). All photons within the Bragg reflection spectral range ΔE_H are almost totally reflected from the crystal and propagate at a scattering angle 2θ with a characteristic delay time $\mathcal{T}_\Lambda = 2\hbar/\Delta E_H$ of Bragg diffraction, as shown in Fig. 2(c). In fact, \mathcal{T}_Λ scales with the characteristic length of Bragg diffraction $\bar{\Lambda}_H$, the so-called extinction length:

$$\mathcal{T}_\Lambda = \frac{2\bar{\Lambda}_H \sin^2\theta}{c|\gamma_H|}, \quad \mathcal{T}_\Lambda \Delta E_H = 2\hbar. \quad (1)$$

Here $\gamma_H = \sin(\eta - \theta)$, and η is an asymmetry angle, see Fig. 2 (left).

Forward Bragg diffraction (FBD) is a multiple coherent scattering of x-rays from the same atomic planes. It is complementary to the BD scattering process. Those spectral components of the incident radiation contribute to FBD, which do not participate in BD, those which are outside but in the immediate vicinity of the Bragg reflection region ΔE_H . The FBD spectral dependence $|R_{00}(E) - R_{00}(\infty)|^2$ in Fig. 2(b) illustrates this. Here $R_{00}(E)$ is a transmission amplitude through the crystal of a spectral component with energy E . The FBD spectral width ΔE_0 scales with the BD spectral width ΔE_H , is larger than ΔE_H , and increases with the crystal thickness d :

$$\Delta E_0 = \Delta E_H \frac{d}{2\pi\bar{\Lambda}_H}, \quad \mathcal{T}_0 = \mathcal{T}_\Lambda \frac{\bar{\Lambda}_H}{d}, \quad \mathcal{T}_0 \Delta E_0 = \frac{\hbar}{\pi}. \quad (2)$$

Respectively, the characteristic time of FBD \mathcal{T}_0 see Fig. 2(c), scales with \mathcal{T}_Λ , is smaller than \mathcal{T}_Λ , and decreases with the crystal thickness.

The FBD crystal response to the excitation by an incident radiation pulse can be calculated as a convolution in time of the incident SASE radiation pulse amplitude $\mathcal{E}_{\text{SASE}}(t)$ and of a forward Bragg diffraction response function G_{00} :

$$\mathcal{E}_0(t) = \int_{-\infty}^t dt' G_{00}(t-t') \mathcal{E}_{\text{SASE}}(t'). \quad (3)$$

Here $\mathcal{E}_{\text{SASE}}(t)$ is a slowly varying envelope. $G_{00}(t)$ presents the crystal response to a delta-function excitation in time and is calculated as a Fourier transform of the FBD spectral amplitudes:

$$G_{00}(t) = R_{00}(\infty) \left[\delta(t) + \tilde{G}_{00}(t) \right] \\ \tilde{G}_{00}(t) = \int_{-\infty}^{\infty} \frac{d\Omega}{2\pi} e^{-i\Omega t} \frac{R_{00}(\Omega) - R_{00}(\infty)}{R_{00}(\infty)}, \quad (4)$$

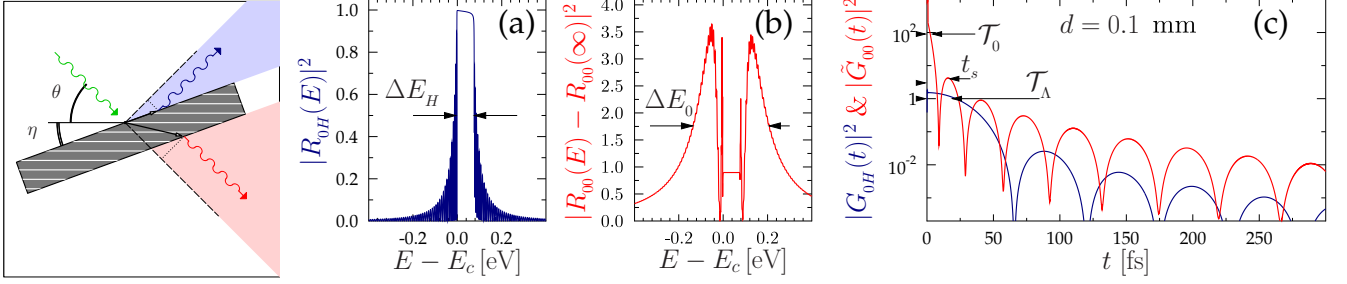


FIG. 2: (Color online) (left) Schematic of Bragg diffraction (BD) and forward Bragg diffraction (FBD) of x-rays from a crystal in Bragg-case geometry. (a) Example of energy dependence of x-ray reflectivity $|R_{0H}(E)|^2$ in Bragg diffraction and (b) of energy dependence of forward Bragg diffraction $|R_{00}(E) - R_{00}(\infty)|^2$ from a diamond crystal in the 004 Bragg reflection, $E_c = 8.33$ keV, $\theta = 56.6^\circ$, $\eta = 0^\circ$, $d = 0.1$ mm. (c) Intensities of corresponding time dependencies of crystal response to an excitation with ultra-short x-ray pulse in BD $|G_{0H}(t)|^2$ (blue) and in FBD $|G_{00}(t)|^2$ (red), respectively.

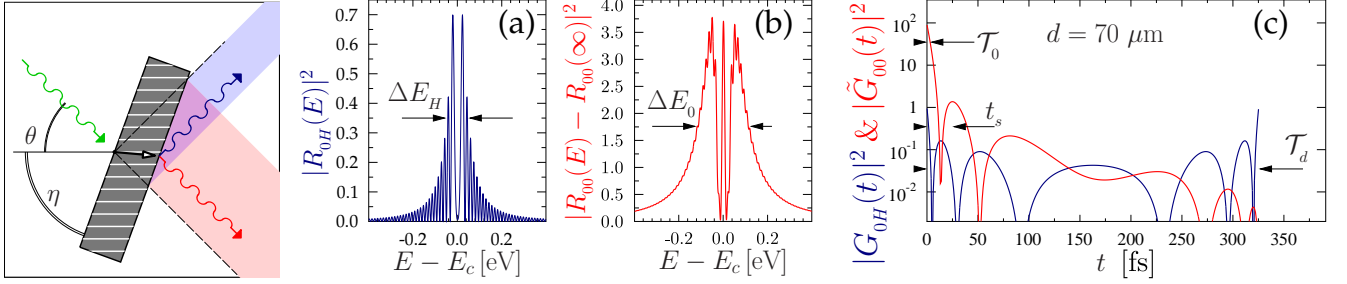


FIG. 3: (Color online) (left) Schematic of Bragg diffraction (BD) and forward Bragg diffraction (FBD) of x-rays from a crystal in Laue-case scattering geometry. All notations are as in Fig. 2. Example of energy and time dependencies from a diamond crystal in the 004 Bragg reflection, $E_c = 8.33$ keV, $\theta = 56.6^\circ$, $\eta = 90^\circ$, $d = 0.1$ mm.

where $\Omega = (E - E_c)/\hbar$. According to Eq. (4), $G_{00}(t)$ is in fact a sum of the prompt, i.e., diffraction-free transmission $R_{00}(\infty)\delta(t)$ of the far-from-Bragg-reflection-region spectral components, and of the delayed *actual* forward diffraction response function $\tilde{G}_{00}(t)$. As a result, the final expression for the time dependence of the radiation field emanating from the crystal in the forward direction

$$\mathcal{E}_o(t) = R_{00}(\infty) \left[\mathcal{E}_{\text{SASE}}(t) + \int_{-\infty}^t dt' \tilde{G}_{00}(t-t') \mathcal{E}_{\text{SASE}}(t') \right] \quad (5)$$

is a sum of the diffraction-free transmitted SASE radiation and of the second component, which is the delayed monochromatic seed due to FBD.

In general, FBD is characterized also by a spatial transverse shift of the delayed radiation emitted by the crystal in the forward direction [3, 15]. In the present studies we will, however, assume for simplicity that the spatial shift of the FBD signal is small and can be neglected.

An analytical expression can be derived for the forward diffraction time response function $\tilde{G}_{00}(t)$ in the approximation of a non-absorbing and thick $d \gg \bar{\Lambda}_H^{(s)}$ crystal valid in the general case of asymmetric Bragg diffraction,

both in Bragg-case geometry (Fig. 2):

$$\tilde{G}_{00}(t) = -\frac{1}{2\mathcal{T}_0} \frac{J_1 \left[\sqrt{\frac{t}{\mathcal{T}_0} \left(1 + \frac{t}{\mathcal{T}_d}\right)} \right]}{\sqrt{\frac{t}{\mathcal{T}_0} \left(1 + \frac{t}{\mathcal{T}_d}\right)}}, \quad (6)$$

and in Laue-case geometry (Fig. 3):

$$\tilde{G}_{00}(t) = \frac{1}{2\mathcal{T}_0} \left(1 - \frac{t}{\mathcal{T}_d}\right) \frac{J_1 \left[\sqrt{\frac{t}{\mathcal{T}_0} \left(1 - \frac{t}{\mathcal{T}_d}\right)} \right]}{\sqrt{\frac{t}{\mathcal{T}_0} \left(1 - \frac{t}{\mathcal{T}_d}\right)}} \quad (7)$$

$$[0 < t < \mathcal{T}_d],$$

with the characteristic time parameters

$$\mathcal{T}_0 = \frac{2[\bar{\Lambda}_H^{(s)}]^2}{c(d/\gamma_0)}, \quad \mathcal{T}_d = \frac{2d \sin^2 \theta}{c|\gamma_H|}. \quad (8)$$

\mathcal{T}_0 is the characteristic time of forward Bragg diffraction, the same as in Eq. (2). Here it is expressed, however, through a Bragg-reflection-invariant – the extinction length $\bar{\Lambda}_H^{(s)}$ in symmetric diffraction geometry ($\eta = 0$) – and by the effective crystal thickness d/γ_0 , the thickness seen by incident x-rays, $\gamma_0 = \sin(\theta + \eta)$. Extinction length $\bar{\Lambda}_H^{(s)}$ values for Bragg reflections in diamond, Si,

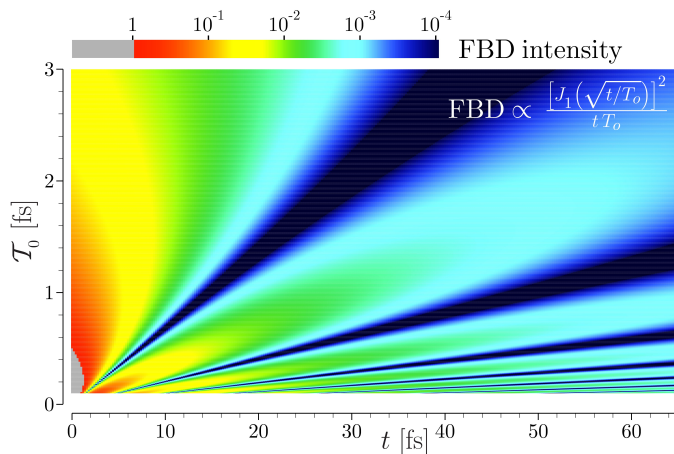


FIG. 4: (Color online) 2D plot of the universal FBD response function intensity $|\tilde{G}_{00}(t)|^2$ (in relative units) plotted for different values of the time delay t to the instantaneous excitation of the crystal, and for different values of the FBD time constant \mathcal{T}_0 , using Eq. (9).

and Al_2O_3 are tabulated in [3, 16]. The parameter \mathcal{T}_d is a characteristic measure of time in Bragg diffraction associated with the crystal thickness d . In the Laue-case geometry, \mathcal{T}_d is equal to the total duration of forward Bragg diffraction, see Fig 4(c). In the Bragg-case geometry, it measures the time between multiple reflections.

If additionally, the delay times of interest are short $t \ll \mathcal{T}_d$ compared to the propagation time through the crystal, a generic expression can be used for all symmetric or asymmetric, Bragg-case or Laue-case geometries:

$$\tilde{G}_{00}(t) = \text{sgn}\{b\} \frac{1}{2\mathcal{T}_0} \frac{J_1\left(\sqrt{t/\mathcal{T}_0}\right)}{\sqrt{t/\mathcal{T}_0}}, \quad t \ll \mathcal{T}_d. \quad (9)$$

The time constant of forward Bragg diffraction \mathcal{T}_0 Eq. (8) is the only parameter that enters Eq. (9), and is the only parameter that defines the strength, delay, and duration of FBD and therefore of the monochromatic seed. The physics is controlled by the parameters that compose \mathcal{T}_0 Eq. (8): the magnitude of the effective crystal thickness d/γ_0 , and the extinction length $\bar{\Lambda}_H^{(s)}$ in the symmetric Bragg reflection. A 2D plot of the FBD intensity $\propto |\tilde{G}_{00}(t)|^2$, in the (t, \mathcal{T}_0) space, shown in Fig. 4, can be used as an initial guide to the most beneficial \mathcal{T}_0 values for seeding at a given time delay t .

The first trailing maximum of $|\tilde{G}_{00}(t)|^2$, which was originally proposed to use as the monochromatic seed, appears at the time delay $t_s = 26\mathcal{T}_0$, see Fig. 2(c). Its duration is $\Delta t_s = 16.5\mathcal{T}_0$. Both the delay and duration can be tailored by changing \mathcal{T}_0 , which can be done practically by adjusting the extinction length $\bar{\Lambda}_H^{(s)}$ (for example, by choosing another reflection or asymmetry parameter), or by changing the crystal thickness.

Table I shows examples of \mathcal{T}_0 and \mathcal{T}_d used in the subse-

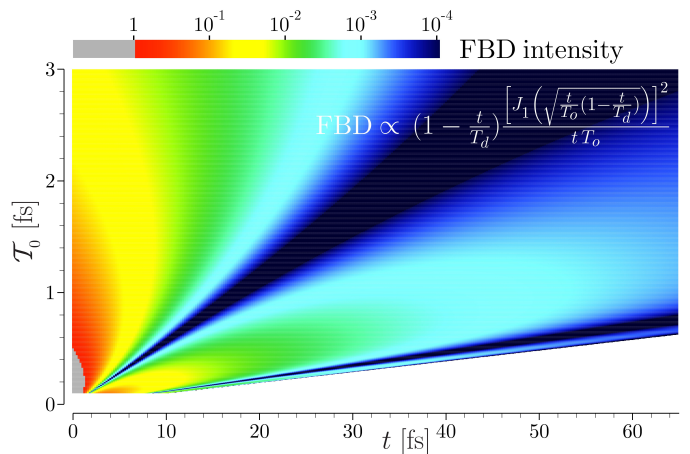


FIG. 5: (Color online) Similar to Fig. (4), however, Eq. 7 for the Laue-case FBD response function is used for a particular case of $\mathcal{T}_d \simeq 104\mathcal{T}_0$, which permits the duration of the FBD peaks to be stretched.

quent simulations and how these values can be realized with particular Bragg reflections. The realization of a particular \mathcal{T}_0 is not unique. The same \mathcal{T}_0 values can be realized with different Bragg diffraction vectors, i.e., different $\bar{\Lambda}_H^{(s)}$, different crystal thicknesses d , and different scattering geometry parameters θ , η , γ_H , and γ_0 .

An interesting situation may occur in Laue-case diffraction. Unlike the Bragg-case diffraction presented by Eq. (6), the argument $a = t/\mathcal{T}_0(1 - t/\mathcal{T}_d)$ of the response

\mathbf{H}	$\bar{\Lambda}_H^{(s)}$	d	θ	η	γ_H	γ_0	\mathcal{T}_0	\mathcal{T}_d	ΔE_0
hkl	μm	μm	deg	deg			fs	fs	meV
111	1.09	40	21.3	0	0.36	-0.36	0.07	94	2993
111	1.09	100	21.3	90	0.93	0.93	0.07	94	
220	1.98	75	36.3	0	0.59	-0.59	0.21	296	998
220	1.98	100	36.3	90	0.81	0.81	0.21	296	
400	3.63	100	56.8	0	0.84	-0.84	0.73	558	287
511	7.83	260	82.9	15.8	0.99	-0.92	1.5	1720	140
511	7.83	130	82.9	15.8	0.99	-0.92	3.0	860	70
511	7.83	100	82.9	15.8	0.99	-0.92	4.1	712	51
511	7.83	58	82.9	15.8	0.99	-0.92	7.0	413	30

TABLE I: Examples of the time constants \mathcal{T}_0 , and \mathcal{T}_d in Eq. (8) used in the subsequent simulations; and their realization through particular (not at all unique) Bragg diffraction cases. The appropriate FBD spectral bandwidths ΔE_0 – Eq. (2) – are also provided for reference. Each Bragg diffraction case is defined first of all by the Bragg reflection invariant diffraction vector \mathbf{H} and symmetric extinction length $\bar{\Lambda}_H^{(s)}$ in diamond crystals, by the crystal thickness d , and by the parameters defining scattering geometry: the Bragg angle θ , the asymmetry angle η , the incidence wave vector projection $\gamma_0 = \sin(\theta + \eta)$ to the crystal internal normal, and the reflection wave vector projection $\gamma_H = \sin(\eta - \theta)$, respectively.

function in the Laue-case diffraction, Eq. (7), attains the maximum value $a_{\max} = \mathcal{T}_d/4\mathcal{T}_0$ at $t_{\max} = \mathcal{T}_d/2$. The argument changes slowly with time around t_{\max} . If in addition $a_{\max} \simeq 26$, i.e., $\mathcal{T}_d/\mathcal{T}_0 = (d/\bar{\Lambda}_H^{(s)})^2 \sin^2 \theta / (|\gamma_H| |\gamma_0|) \simeq 104\mathcal{T}_0$, the first trailing maximum of the response function will be stretched in time compared to the Bragg-case FBD, as graphically shown in Fig. 5. This property maybe useful for seeding long electron bunches.

B. Single-Color and Multi-Color Seeding Conditions

The FBD spectra presented in Figs. 2(b) and 3(b) are time integrated. The actual spectrum of the radiation that seeds the electron bunch is related to it, but not identical, as the electron bunch “sees” only a part of the FBD signal. The seeding radiation spectrum is determined by the Fourier transform of the product of the FBD amplitude $\mathcal{E}_0(t)$ - Eq. (5), and of the electron current time profile. Examples of seeding radiation spectra, calculated for an idealistic case of prompt excitation $\mathcal{E}_{\text{SASE}}(t) \propto \delta(t)$ and for an electron bunch with Gaussian profile are shown in Fig. 6. The radiation spectrum that seeds the electron bunch depends largely on the relationship between the electron bunch duration σ_e and the time profile of the radiation overlapping with the electron bunch. The latter can be varied either by the FBD time constant \mathcal{T}_0 or/and by the electron bunch delay τ_e .

In the limiting case of a flat time profile, the seeding spectrum is defined by σ_e and will have a spectral width of $\simeq \hbar/\sigma_e$. This spectral width represents the finest spectral feature that the XFEL system can generate. This is also a typical spectral width of the spikes in the SASE spectra [10, 17].

Therefore, if the FBD spectral width is chosen to be $\Delta E_0 \simeq \hbar/\sigma_e$, i.e., $\sigma_e \simeq \pi\mathcal{T}_0$, as in the case presented in Fig. 6(a), a close to optimal condition for single-color seeding can be achieved.

In the other limiting case, $\Delta E_0 \gg \hbar/\sigma_e$, i.e., $\sigma_e \gg \pi\mathcal{T}_0$, the FBD time profile has a few oscillations superimposed on the electron bunch. As a result, the seeding spectrum will have a double-peak structure with the separation between the peaks inversely proportional to the oscillation period, i.e., to $\propto 1/\mathcal{T}_0$. This case is presented in Fig. 6(b). The FBD spectrum seen by the electron bunch changes dramatically with time. At small time delays the two outer broader peaks of the FBD spectrum dominate. At larger time delays, the two narrow spectral peaks survive and represent the seeding spectrum. In any case, at any time, the double-peak structure persists, a prerequisite for the two-color seeding. For this, however, appropriate spectral components should also be present in the SASE

spectrum. Due to the stochastic nature of the SASE spectrum, this likely will not always be the case. The XFEL output will result in a two-color output, however, with the spectral content varying from shot to shot.

The Laue-case FBD spectrum can be more fine-structured, see Fig. 3(b). This may provide conditions for more than two-color seeding, i.e., multi-color seeding. Even more important, in the Laue-case geometry the fine structure may have a single narrow peak in the center (unlike the Bragg-case, which always has a double-hump structure); this could be beneficial for a true single-color seeding, as the broad-band spectral components decay fast, leaving only the sharp spectral component for single-color seeding.

III. 3D FEL SIMULATION DETAILS

The 3D time-dependent FEL simulation code GENESIS 1.3 [14] is applied to study XFEL self-seeding with the FBD (wake) monochromator. The main FEL parameters used in the simulations are presented in Table II. They are based on the LCLS commissioning results [18]. Two magnetic undulator systems are used, both with the nominal undulator period $\lambda_w = 30$ mm. The length of the first undulator system U1 is chosen to ensure FEL operations in the exponential growth regime and to achieve the x-ray seed power after the monochromator about two orders of magnitude larger than the shot noise power P_n . At the same time, the U1 length is limited to 60 m to avoid energy spread growth due to FEL saturation. The second undulator system U2 is chosen to be 70 m long for the FEL to reach saturation with reduced fluctuations of the x-ray pulse power. The lengths of the first and the second magnetic undulator systems include the gaps between the undulator sections. A weak four-dipole chicane with $R_{56} \simeq 3 - 45 \mu\text{m}$ is installed in a 4-m-long space between the U1 and U2 undulator systems.

There are typical shot-to-shot SASE radiation fluctuations after the U1 undulator system. As a result, the power and phase of the radiation after the monochromator fluctuates as well, as shown in Fig. 7. See also the discussion in [15]. The power fluctuations could be about 50%. There is a $\simeq 10 - 15$ -fs jitter in the duration and in the form of the SASE signal, resulting in a similar jitter of the seed oscillation peak positions and of the seed phase. The phase time dependences appear to be very different from shot to shot, which is related to how the convolution of a particular SASE radiation pulse with the crystal response function works, see Eq. (5). For realistic FEL output, averaging is required over many shorts. The averaged picture, however, may obscure the underlying physics. For this reason, the following analysis is performed without averaging, but using instead a single typical SASE radiation pulse for all cases. In particular, the SASE pulse, which produces the seed with 2.44 μJ

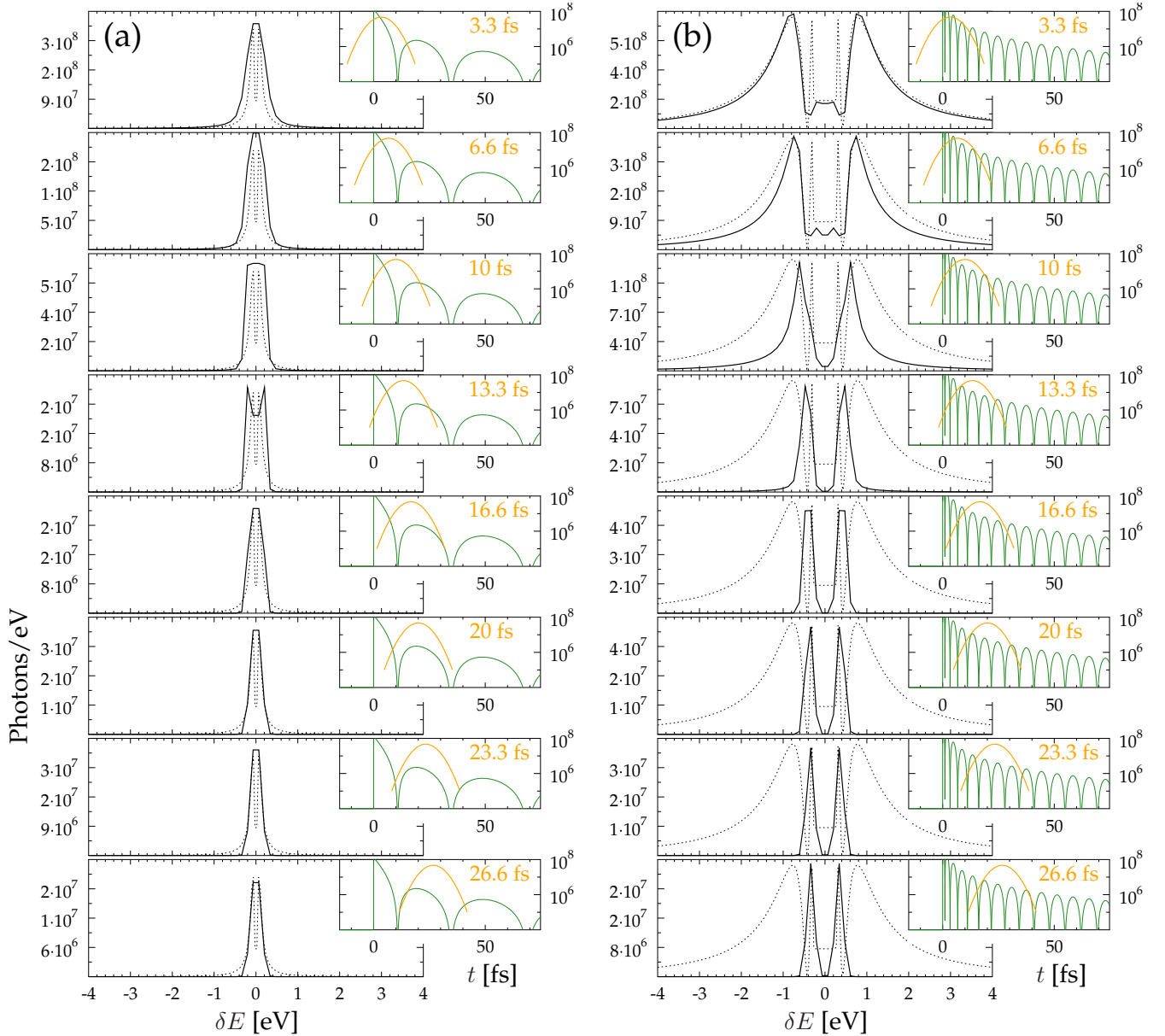


FIG. 6: (Color online) Spectra of the seeding radiation as “seen” by the electron bunch (solid black lines). The spectra are calculated for different delays τ_e of the electron bunch (solid orange lines in the insets) with respect to the FBD intensity (solid green lines in the insets). The dotted lines show for reference the time-integrated FBD spectra. Calculations are presented for an electron bunch with an rms duration $\sigma_e = 5.3$ fs, Bragg-case FBD time constant $\mathcal{T}_0 = 0.75$ fs (a), and $\mathcal{T}_0 = 0.07$ fs (b), respectively. Case (a) with $\mathcal{T}_0 \simeq \sigma_e/\pi$ is optimal for the single-color seeding, while case (b) with $\mathcal{T}_0 \ll \sigma_e/\pi$ is better suited for the two-color seeding.

energy in Fig. 7 is used in the long-bunch simulations.

The FEL calculations are performed within a $6\sigma_e$ time window, where σ_e is the rms duration of the electron bunch. The current and energy distributions along the electron bunch are assumed to be Gaussian. Calculations in the U2 FEL system are performed using a fresh bunch, so as not to obscure the self-seeding effects by additional energy spread after the U1 FEL system. Using a fresh

bunch in the U2 FEL system is actually a very attractive option from many points of view. Use of the fresh bunch has been discussed in the two-electron-bunch self-seeding scheme [13].

The orange lines in Figs. 8, 9, 10, and 11 show the electron current profile within this time range. The dashed cyan lines represent the SASE radiation output after U1 undulator system within the same time window. The

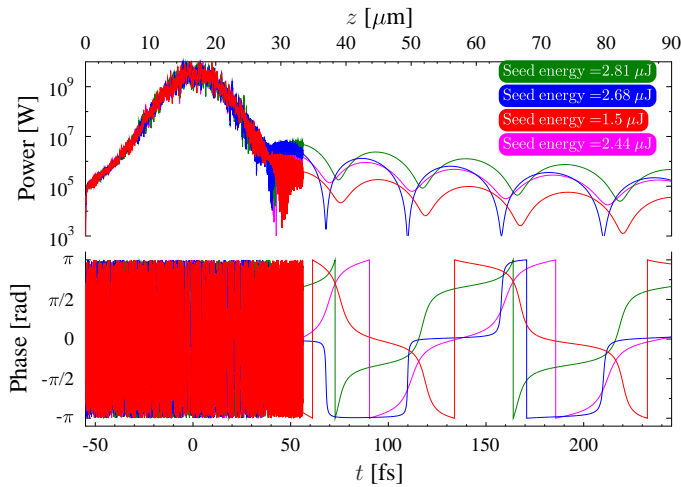


FIG. 7: (Color online) Time dependencies of power and phase of the entire radiation interacting with the electron bunch at the beginning of the U2 undulator system. The entire radiation comprises both the SASE radiation (the first term of Eq. (5)), and the monochromatic seed generated by FBD of the SASE radiation from a crystal (the second term of Eq. (5)). Examples of different SASE pulses in the FEL long-pulse operation mode are shown, demonstrating jitter in the seed power, and positions of the seed maxima. The crystal monochromator with $\mathcal{T}_0 = 0.75$ fs is used.

Parameter & Symbol	Long-bunch mode	Short-bunch mode	Unit
Electron energy E_e	14.3	13.6	GeV
Bunch charge	150	40	pC
Peak current I_e	3	3	kA
Slice energy spread	2.8	5.6	MeV
Slice emittance	0.4	0.4	μm
Bunch duration σ_e	20 (rms)	5.3 (rms)	fs
Bunch duration Δt_e	47 (FWHM)	12.5 (FWHM)	fs
U1 length	60	60	m
U2 length	70	70	m
Undulator period λ_w	30	30	mm
Normalized undulator parameter a_w	2.4729	2.4729	

TABLE II: Main XFEL parameters in self-seeding mode with two magnetic undulator systems U1 and U2, and with a FBD monochromator.

solid magenta lines represent the pure monochromatic seed - the intensity of the second term in Eq. (5), calculated for FBD with different \mathcal{T}_0 values. The dashed blue lines represent the entire radiation, the sum of the SASE and of the monochromatic seed, i.e., everything that enters the U2 undulator system. The phase of the seed is shown in the graphs in the β -rows of Figs. 10 and 11.

The seeded power at the end of the U2 FEL system is very sensitive to the normalized undulator parameter $a_w = (e/mc)(B_w/2k_w)$. Variation by 0.06% from the

optimal value $a_w = 2.4729$ results in a more than 50% drop of power in the long-bunch mode. Parameter a_w is defined by the on-axis undulator field amplitude B_w , the undulator wave number $k_w = 2\pi/\lambda_w$, the electron rest mass m , and the elementary charge e .

A. Short-bunch mode

We first validate the method by using the short electron bunch. The wake-field effects from the undulator chamber are ignored. The main XFEL parameters are shown in Table II.

Figure 8 shows an example of calculations with a monochromatic seed produced by filtering the SASE radiation through the FBD monochromator with the FBD time constant $\mathcal{T}_0 = 0.21$ fs. Such a time constant would correspond, in particular, to the 220 Bragg reflection of the 8.3-keV x-rays from a $d = 75 - \mu\text{m}$ -thick diamond crystal in the symmetric Bragg-case geometry with an asymmetry angle of $\eta = 0$, a Bragg angle of $\theta = 36.3^\circ$, and an extinction length of $\bar{\Lambda}_H^{(s)} = 1.98 \mu\text{m}$. See Table I.

The top left graph of Fig. 8, shows electron bunch current profile (orange line), SASE power (dashed cyan line), seed power (magenta solid line), and the total radiation power (dashed dark blue line). The right top graph shows the time-integrated spectral density of the seed after the monochromator. It is a product of the FBD spectrum, the kind of spectrum shown in Fig. 2(b), with a noisy SASE spectrum.

The graphs in the lower rows show time dependencies of the XFEL radiation power (left) and spectral densities of the XFEL radiation (right), calculated for different electron bunch delays τ_e . The spectral dependencies are shown in a range much narrower than the SASE spectrum width, to emphasize details of the seeded spectrum. The bandwidths of the seeded spectra are narrower than the spectrum of the seed, and change with the delay τ_e . We will present and discuss the results of the simulations in detail in Sec. IV.

B. Long-bunch mode

Having validated the simulations in the short-bunch mode, we apply the procedure to the long-bunch mode. The current and energy distributions along the bunch are also Gaussian. For simplicity, the wake-field effects due to the resistive wall impedance of the undulator chamber are not considered here as well.

In the short-bunch mode, the wake-field effects are negligible. However, in the long-bunch mode, they may induce a substantial energy chirp along the electron bunch,

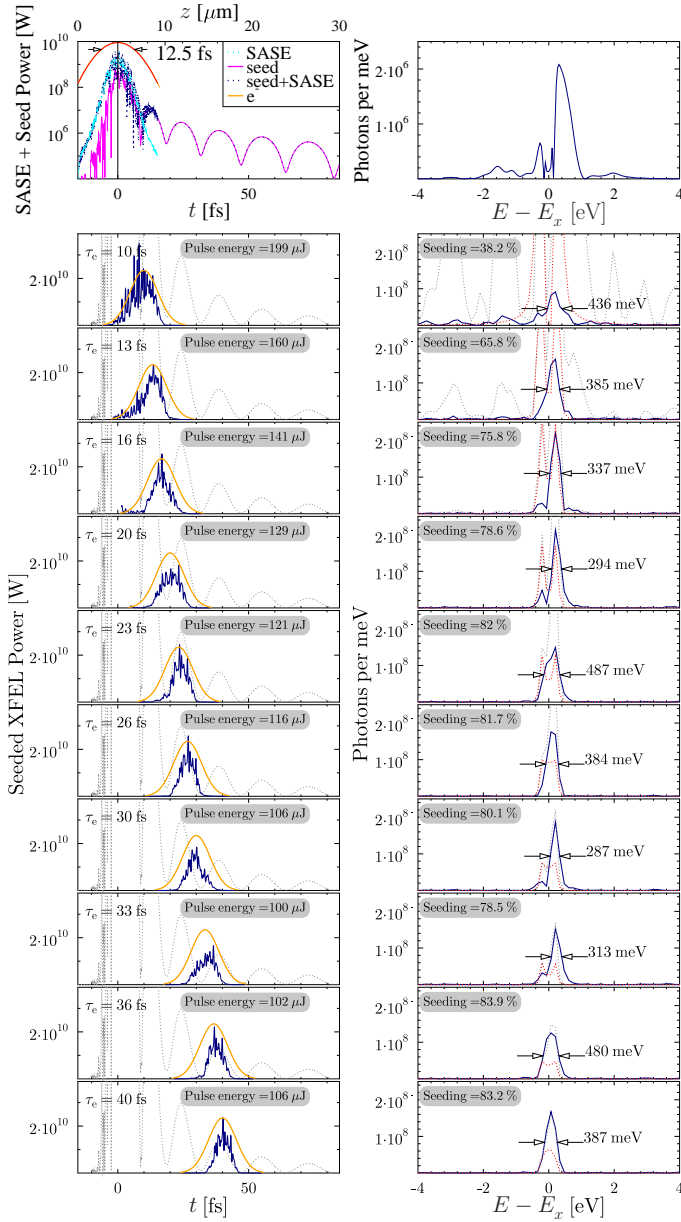


FIG. 8: (Color online) Time (left) and spectral (right) dependencies of the XFEL radiation in the self-seeding short-bunch mode. Graphs in the top row, present the dependencies at the entrance of the U2 undulator system. Seeding is performed by the FBD monochromator with the FBD time constant $\mathcal{T}_0 = 0.21$ fs. The top right spectrum of the seeding radiation is time-integrated. The lower graphs show in solid dark blue lines the time and spectral dependencies at the end of the U2 system for different electron bunch delays τ_e . Orange lines show the electron current profiles. The dashed gray lines in the left graphs are the time profile of the seed. The dashed gray lines in the right graphs represent the seed spectrum as it is “seen” by the electron bunch at appropriate time delays. Red dashed lines show the same, however, for an idealistic case of instantaneous excitation of the crystal with a white spectrum. The nominal photon energy $E_x = 8.3$ keV.

move electrons off the FEL interaction bandwidth, and

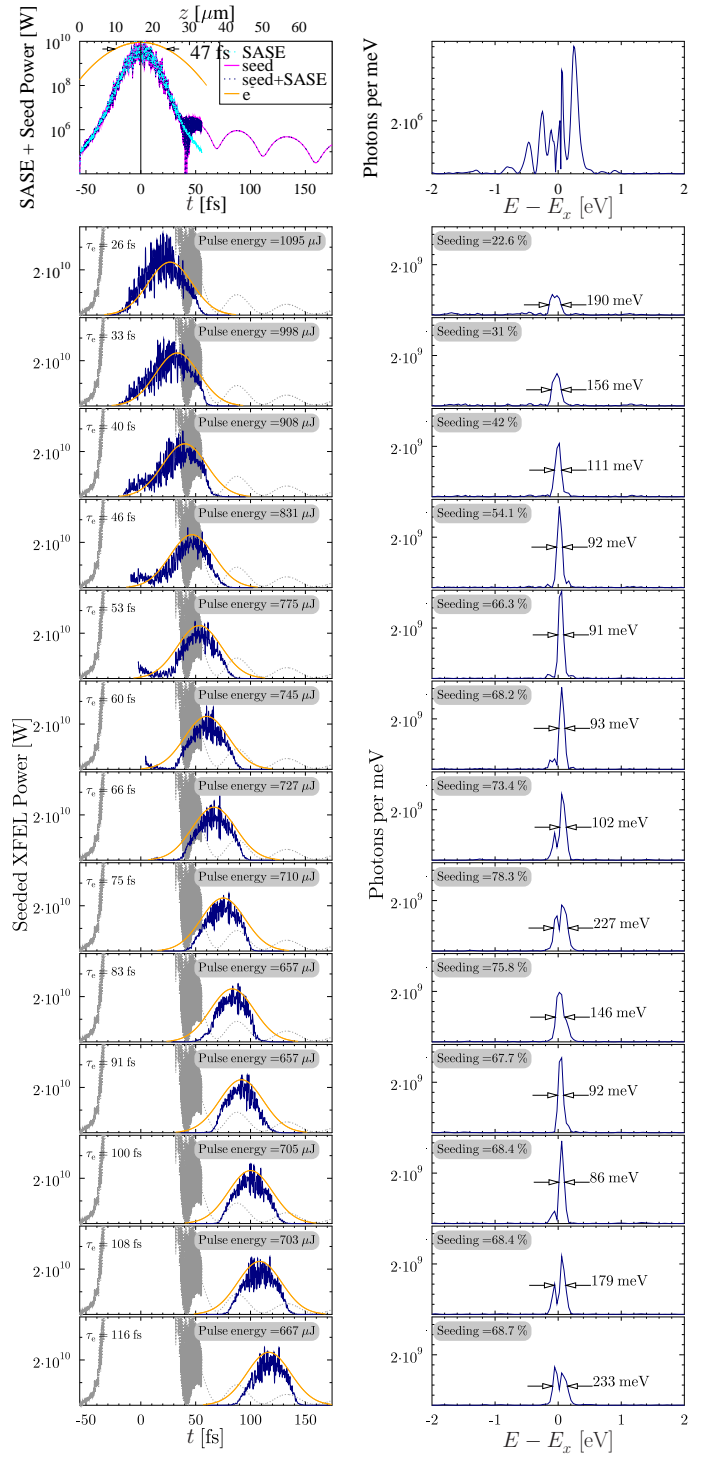


FIG. 9: (Color online) Similar to Fig. 8, however, showing results of calculations in the long-bunch mode, with seeding by the FBD monochromator with the FBD time constant $\mathcal{T}_0 = 0.75$ fs. The nominal photon energy $E_x = 9.1$ keV.

thus degrade the seeding efficiency. There are several techniques, such as electron bunch pre-chirp [19], specially shaped vacuum chamber [20], etc., that could be used to mitigate the wake-field effects.

Parameter & Symbol	Long-bunch mode	Short-bunch mode	Unit
Photon energy E_x	9.10	8.30	keV
Wavelength	1.36	1.50	Å
SASE radiation after U1			
SASE pulse energy	83	9	μJ
SASE peak power	3	1.2	GW
Seeded radiation after U2			
Pulse peak power	20	15	GW
Photons per pulse	4×10^{11}	8×10^{10}	
Pulse energy	680	100	μJ
Pulse duration Δt_x	34 (FWHM)	8 (FWHM)	fs
Pulse duration σ_x	15 (rms)	3.5 (rms)	fs
Min. bandwidth ΔE_x	90 (FWHM)	320 (FWHM)	meV
Min. bandwidth σ_{E_x}	38 (rms)	136 (rms)	meV
Max. spectral flux F_m	$\simeq 3 \times 10^9$	$\simeq 2 \times 10^8$	ph/meV
F_m per pC, \bar{F}_m	$\simeq 2 \times 10^7$	$\simeq 6 \times 10^6$	ph/meV/pC

TABLE III: \mathcal{T}_0 -independent XFEL radiation parameters in self-seeding mode with FBD monochromators. By “seeded radiation” we define the portion of the total radiation enclosed within the narrow bandwidth, as a result of self-seeding process.

Figure 9 shows an example of calculations with a monochromatic seed produced by filtering the SASE radiation through the FBD monochromator with the FBD time constant $\mathcal{T}_0 = 0.75$ fs. Such time constant could be realized in different ways, one of them presented in Table I: by using the 004 Bragg diffraction of the 9.1 keV x-rays from a $d = 100$ μm thick diamond crystal in the symmetric Bragg-case geometry with an asymmetry angle $\eta = 0$, a Bragg angle of $\theta = 56.8^\circ$, and an extinction length of $\bar{\Lambda}_H^{(s)} = 3.63$ μm.

One of striking features, of the data presented in Fig. 9, is that the substantial variation of the seeded radiation bandwidth with the electron bunch delay τ_e . We will present and discuss the results of the simulations in detail in Sec. IV.

IV. RESULTS AND DISCUSSION

The seeded XFEL radiation characteristics for different seeding conditions are presented graphically in the long-bunch mode in Fig. 10 and in the short-bunch mode in Fig. 11. The seeding conditions are varied by changing FBD time constant \mathcal{T}_0 and the electron bunch delay τ_e . The results for different \mathcal{T}_0 are shown in the appropriate columns of Figs. 10 and 11. The XFEL radiation characteristics (the focus is on spectral properties) such as peak power, total number of photons, total number of seeded photons, x-ray pulse duration, spectral bandwidth, and

spectral line center position are presented as a function of the electron bunch delay τ_e by the graphs in respective rows of Figs. 10 and 11. \mathcal{T}_0 -independent characteristics of the XFEL radiation are presented in Table III.

The main observations, which can be derived from the results presented in Figs. 10 and 11, are summarized below.

A. Peak Power

The peak power of the radiation pulse at the end of the XFEL is stable, and independent of \mathcal{T}_0 and of the electron bunch delay τ_e . See graphs in the γ -rows. It has approximately the same magnitude, both in the short-bunch and in the long-bunch modes. Still, it is slightly larger in the long-bunch mode. This is consistent with the FEL theory, see Eq. (91) of [10], predicting the saturation power level $P_{\text{sat}} \propto \rho P_{\text{beam}}$ to be a fraction of the total electron beam power $P_{\text{beam}} = E_e I_e / e$, with the fraction given by the dimensionless Pierce parameter ρ [7], which is typically $\simeq 10^{-3}$. The peak current I_e and ρ values are the same in both cases, however, the electron energy E_e is chosen larger in the long-bunch mode, see Table II.

B. Number of Photons per Pulse

The total number of photons per pulse changes with the delay τ_e . It is the largest at smaller delays, where the SASE contribution is the largest, see graphs in the δ -rows of Figs. 10 and 11. On average, the total number of photons is four times larger in the long-bunch mode, which corresponds to a four times larger pulse duration and four times larger charge in the long-bunch compared to the short-bunch mode.

We are interested primarily in the total number of “seeded photons”, those condensed in a narrow bandwidth, as a result of the self-seeding process. The bandwidth may change with \mathcal{T}_0 , as seen in the right columns of Figs. 8 and 9. The total number of seeded photons within a band defined as the four smallest bandwidths is shown by red circles in δ -row-graphs of Figs 10, and 11. The total number of seeded photons is largest for those electron bunch delays τ_e at which the electron bunch is seeded with the radiation (magenta lines in the α -row graphs of Figs. 10 and 11) whose power is much larger than the shot-noise power P_n level. Dashed black lines in the α -row graphs of Figs. 10 and 11 show the $10 \times P_n$ level. The effective shot-noise power is estimated to be $P_n \simeq \rho^2 E_e E_x / h\sqrt{2\pi} \simeq 14$ kW [8, 10].

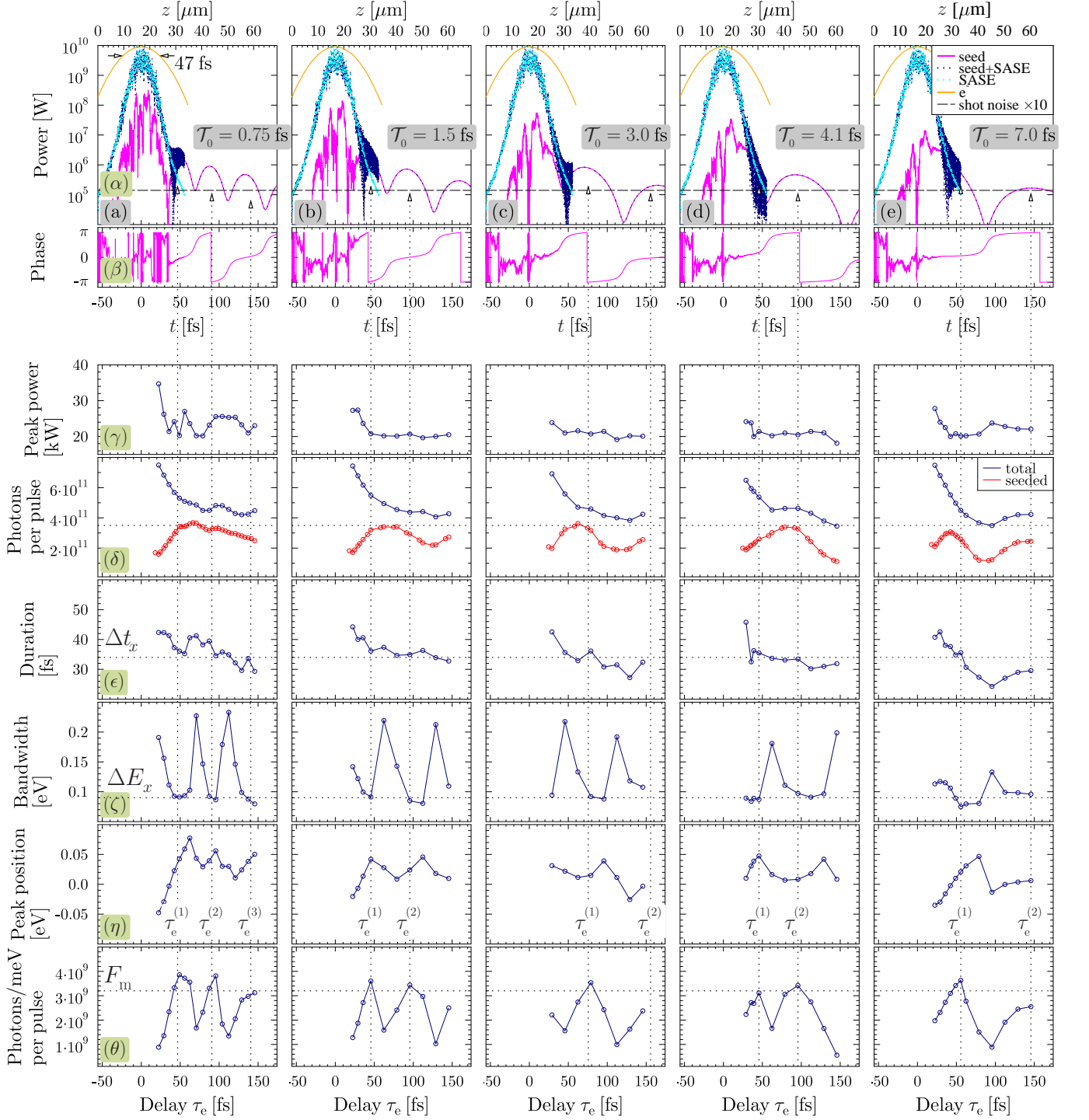


FIG. 10: (Color online) Time dependencies of the monochromatic seed power (magenta lines in the α -row graphs), seed plus SASE power (dashed blue line in same graphs), ten times increased shot-noise level (dashed black line), and the time dependencies of the seed phase – graphs in the β -row. The seed is generated in the long-bunch mode by a SASE radiation from the U1 undulator system (cyan lines in the α -row graphs) in forward Bragg diffraction (FBD) from crystals with FBD time constant $\mathcal{T}_0 = 0.75$ fs (a), $\mathcal{T}_0 = 1.5$ fs (b), $\mathcal{T}_0 = 3.0$ fs (c), $\mathcal{T}_0 = 4.1$ fs (d), $\mathcal{T}_0 = 8$ fs (e). Graphs in other rows represent properties of the radiation at the end of the undulator system U2, as a function of the electron bunch delay τ_e in the magnetic chicane.

C. Pulse Duration

The duration of the x-ray pulse Δt_x (FWHM) is shorter than the duration of the electron bunch; see Figs. 8 and 9,

and the graphs in the ϵ -rows of Figs. 10 and 11. This fact reflects the non-linear nature of lasing physics, in which

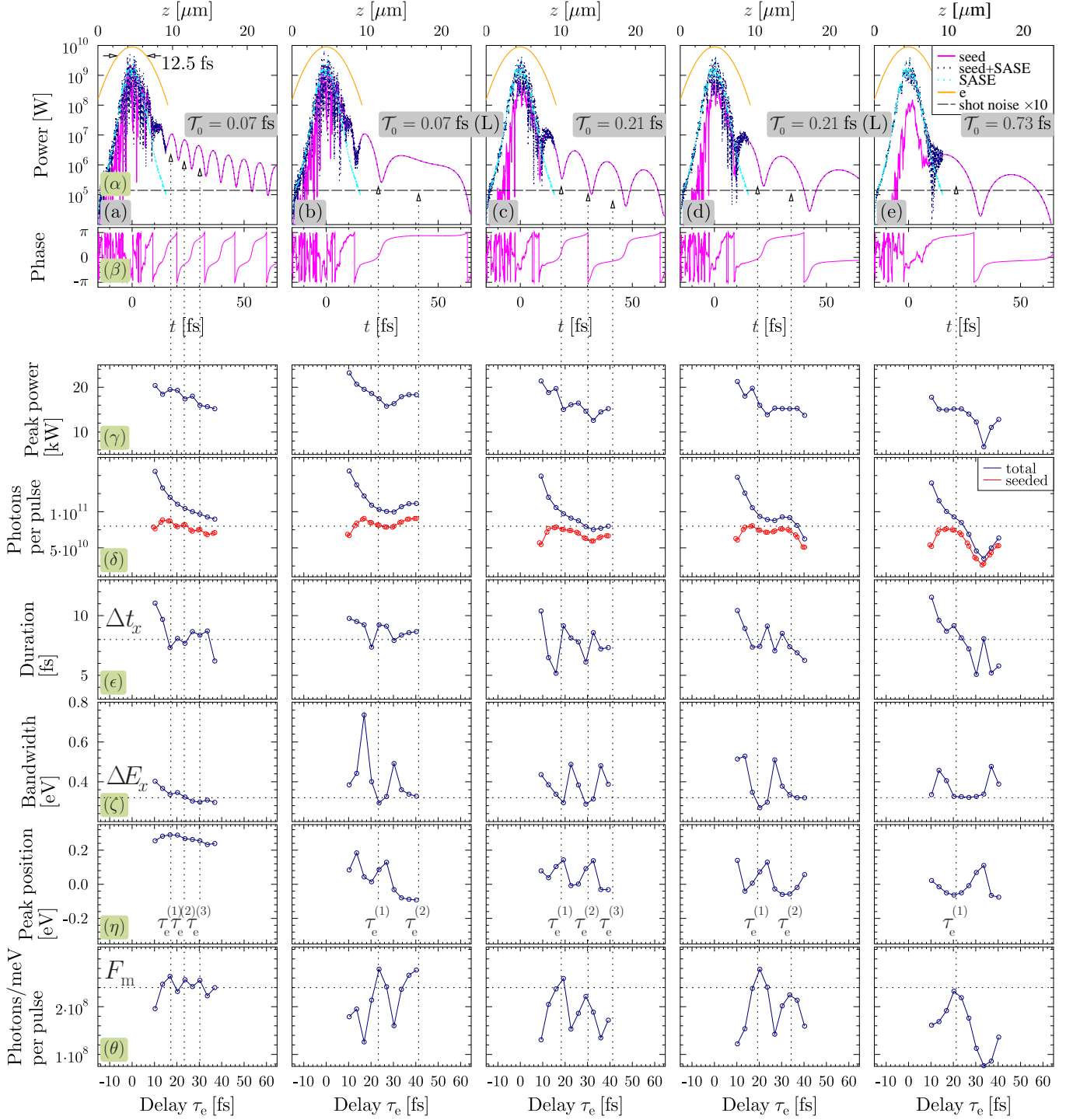


FIG. 11: (Color online) Same as Fig. 10, but for the short-bunch mode calculations with (a) $\mathcal{T}_0 = 0.07$ fs (Bragg-case), (b) $\mathcal{T}_0 = 0.07$ fs (Laue-case), (c) $\mathcal{T}_0 = 0.21$ fs (Bragg-case), (d) $\mathcal{T}_0 = 0.21$ fs (Laue-case), (e) $\mathcal{T}_0 = 0.73$ fs (Bragg-case).

the high-current portion of the electron bunch produces the most significant effect.

D. Spectral Bandwidth

The spectral bandwidth of the radiation achieves its smallest values ΔE_x (FWHM) at specific electron bunch delays $\tau_e^{(n)}$, with respect to the monochromatic seed, indicated by vertical dashed lines with arrows; see the ζ -

row graphs in Figs. 10 and 11. The smallest achievable bandwidth ΔE_x is practically independent of \mathcal{T}_0 . However, it takes different values in the long-bunch and in the short-bunch modes.

The product $\sigma_x \sigma_{E_x} \approx 5 \times 10^{-16}$ eV·s of the rms x-ray pulse duration, and the rms minimal x-ray pulse bandwidth, is very close to Planck's constant $\hbar = 6.6 \times 10^{-16}$ eV·s. This suggests that self-seeding results in the almost Fourier-transform limited, i.e., in the fully longitudinally coherent, FEL radiation. This also very clearly suggests that the ultimate spectral properties of the self-seeding XFEL are determined first of all by the length σ_e of the electron bunch rather than by the properties of the radiation seed. The seed helps to achieve the best performance; however, it does not determine the final result.

The bandwidth may increase by a factor of three from its smallest value if the electron bunch delay is chosen somewhere between the specific delays $\tau_e^{(n)}$; see Fig. 10(η). The larger \mathcal{T}_0 is, the broader are the τ_e intervals where the smallest bandwidth values are attained. Because of the jitter in the SASE radiation, resulting in a jitter of the positions and of the seed power peaks and phase (see Fig. 7), it may be more advantageous to choose FBD with longer \mathcal{T}_0 values, to achieve stable self-seeding with narrowest bandwidth and highest spectral flux, independent of SASE jitter. At the same time adequate seed power should be ensured as well. FBD with too long a \mathcal{T}_0 may produce insufficient seed power. The optimal value is $\mathcal{T}_0 \simeq \sigma_e/\pi$, as was discussed in Sec. II B. FBD with a very short $\mathcal{T}_0 \ll \sigma_e/\pi$ may result in double-color seeding.

E. Double-Color Seeding

Double-color seeding in the long-bunch mode is shown in Fig. 12, with an FBD monochromator having $\mathcal{T}_0 = 0.07$ fs. We note that the double-color seeding with equal intensities of both colors, as shown in Fig. 12, cannot be achieved in each XFEL shot. Our simulations show that the relative intensity variations of the two colors take place from shot to shot. The success for equal-intensity double-color seeding depends on the spectral composition of the SASE spectrum. Only if both sharp peaks of the FBD spectrum, as in Fig. 6(b), are “populated”, equal-intensity double-color seeding does take place. The total power of the seeded radiation is the same as in single-color seeding; however, it is shared between the two spectral components.

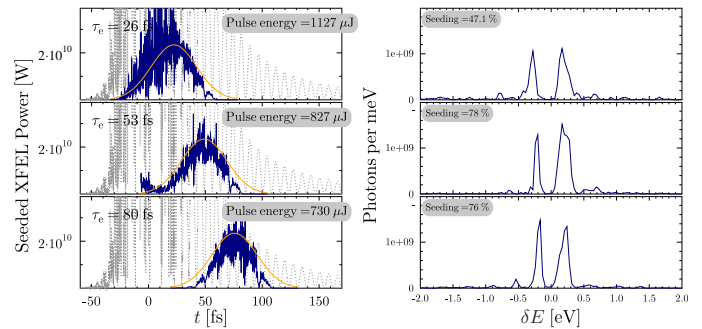


FIG. 12: (Color online) Time (left) and spectral (right) dependencies of the XFEL radiation in the self-seeding long-bunch mode with the FBD monochromator having $\mathcal{T}_0 = 0.07$ fs. The graphs show in solid dark blue lines the time and spectral dependencies at the end of the U2 system for different electron bunch delays τ_e . Orange lines show the electron current profiles. The dashed gray lines in the left graphs are the time profiles of the seed. The nominal photon energy $E_x = 9.1$ keV.

F. Spectral Line Center Position

The center of the self-seeding XFEL output spectrum varies with the electron bunch delay, as shown in the η -row graphs of Figs. 10 and 11. The variation is not pronounced; however, it correlates with the time structure of the monochromatic seed.

A considerable shift of $\simeq +0.2$ eV of the peak position in the $\mathcal{T}_0 = 0.07$ -fs Bragg case in the short-bunch mode is due to the fact that this is actually the double-color seeding case. There are actually two sharp peaks in this case FBD seeding spectrum, as in Fig. 6. However, for the particular SASE spectrum used in these simulations, only one of the two peaks is “populated”.

G. Spectral Flux

In each mode, the maximum spectral flux F_m (measured in photons/pulse/meV) is independent of \mathcal{T}_0 ; see the η -row graphs in Figs. 10 and 11. In the long-bunch mode $F_m \simeq 3.2 \times 10^9$ ph/meV/pulse, while in the short-bunch mode it is an order of magnitude smaller – $F_m \simeq 2.2 \times 10^8$ ph/meV/pulse. The spectral flux values, normalized to the total bunch charge, are $\bar{F}_m \simeq 2.1 \times 10^7$ ph/meV/pC/pulse in the long-bunch mode and $\bar{F}_m \simeq 0.55 \times 10^7$ ph/meV/pC/pulse in the short-bunch mode, respectively, and differ by a factor of four. For comparison, an XFEL in the oscillator configuration produces $\bar{F}_m \simeq 2 \times 10^7$ ph/meV/pC/pulse [21], the number close to the high-gain XFEL in the long-bunch mode considered here.

The maximum spectral flux is attained at the same specific electron bunch delays $\tau_e^{(n)}$ at which the smallest spectral bandwidth is achieved. These delays correlate but do not always coincide with the seed power peaks in the α -row graphs. The delays τ_e are systematically shifted to later times from the peaks' positions. This is clearly seen especially in the short-pulse mode examples in Fig. 11.

The efficient seeding can be performed by using the first or second trailing peaks of the FBD radiation, as discussed in this paper and in the literature [1, 2]. However, it also can be performed efficiently by using the zeroth maximum of the FBD radiation, as the case of $\mathcal{T}_0 = 7$ fs in the long-bunch mode in Fig. 10(η) demonstrates, with the delay set at $\tau_e \simeq 50$ fs.

Figure 11(η), for $\mathcal{T}_0 = 0.07$ fs, shows an exceptional case of seeding, resulting in high spectral flux and smallest bandwidth practically *independent* of the delay τ_e . This does not fit into the general picture discussed until now. Indeed, this is achieved under exceptional conditions, when the period of the FBD power oscillations is much shorter than the electron bunch duration, i.e., under the conditions where double-color seeding is expected. As was already mentioned in Sec. IV F, there are actually two sharp peaks in the FBD seeding spectrum in this case, as in Fig. 6. However, the particular SASE spectrum used in the simulations has spectral components which "populate" only one of the of the two FBD peaks.

The case $\mathcal{T}_0 = 0.07$ fs proves again that a strong seed will produce a stable τ_e -independent output with the spectral flux and spectral width defined eventually by the XFEL parameters, rather than by the seed properties.

In Sec. II we have stated that for time delays $t \ll \mathcal{T}_d$, the Bragg-case and Laue-case FBDs are equivalent and are defined by a single parameter – the FBD time constant \mathcal{T}_0 ; see Eq. (9). At longer times, however, Bragg-case and Laue-case FBDs are not equivalent, and have to be described by different equations (6) and (7), respectively, with the time constant \mathcal{T}_d taken into account. Examples of the $\mathcal{T}_0 = 0.07$ fs Bragg-case and the $\mathcal{T}_0 = 0.07$ fs Laue-case, in the short-bunch mode, with $\mathcal{T}_d = 94$ fs (see Table I), demonstrate substantial differences between the two cases already for time delays $t > 30$ fs. Bragg-case FBD results in double-color seeding. On the contrary, Laue-case FBD ensures single-color seeding with very good, if not the best, results for spectral density and spectral width, due to a strong signal and large duration of the seed at $t = 40$ fs.

V. APPLICATIONS

Self-seeding XFELs can generate fully coherent x-ray pulses with a very high spectral flux, much higher than

the state-of-the-art storage ring-based synchrotron radiation sources. Their supreme spectral properties will expand the science reach of the XFELs and stimulate the utilization of advanced high-resolution spectroscopic techniques.

A self-seeding XFEL, in the long-bunch mode considered in this paper, can generate in each pulse $\simeq 2.4 \times 10^{11}$ photons concentrated within an 80-meV broad (FWHM) line, or $\simeq 2.9 \times 10^9$ photons/meV. With the 120-Hz repetition rate of the LCLS machine, the average number of photons that can be generated in an 80-meV broad (FWHM) line is $\simeq 2.8 \times 10^{13}$ photons/s, corresponding to a spectral flux of $\simeq 3.5 \times 10^{11}$ photons/s/meV. This spectral flux number is an order of magnitude larger than an average spectral flux available at the 3rd generation storage ring-based machines such as ESRF, APS, or SPring-8. The future high-repetition-rate XFELs, such as the European XFEL [22], with an average 30-kHz pulse rate, will be able to generate a spectral flux of $\simeq 8.7 \times 10^{13}$ photons/s/meV, i.e., approximately three orders of magnitude more than the average spectral flux available presently at the synchrotron radiation facilities.

High-resolution inelastic x-ray scattering (IXS) and resonant IXS (RIXS) spectroscopies, widely used for studies of collective excitation in condensed matter [23–25], will tremendously benefit from x-ray sources with largely enhanced average and peak spectral flux. In particular, applications of IXS and RIXS spectrographs working with 9-keV photons [26, 27] will permit studies with spectral resolution better than 0.1 meV. X-ray sources with largely enhanced average spectral flux would be also attractive for other high-spectral-resolution tools, such as nuclear resonance (Mössbauer) spectroscopies [28, 29], as was discussed, in particular, in the first paper on hard x-ray self-seeding [12].

VI. CONCLUSIONS

We have performed theoretical studies for the best conditions under which stable self-seeding of the hard x-ray FEL can be achieved with smallest shot-to-shot variations of the output radiation, with narrowest bandwidth, and largest spectral flux. Characteristic time \mathcal{T}_0 of forward Bragg diffraction (FBD) in the x-ray monochromator crystal determines the power, spectral, and time characteristics of the FBD monochromatic seed. For a given electron bunch duration σ_e the spectral flux of the self-seeding XFEL can be maximized, the spectral bandwidth can be respectively minimized, by choosing $\mathcal{T}_0 \sim \sigma_e/\pi$, and by optimizing the electron bunch delay τ_e . The choice of \mathcal{T}_0 and τ_e is not unique. In all cases, the maximum value of the spectral flux and the minimum bandwidth are primarily determined by the electron bunch length σ_e . The longer the electron bunch, the higher spectral flux can be achieved. It is important,

however, that the power of the seed is about two orders of magnitude larger than the shot noise power, which calls for using FBD monochromators with smaller \mathcal{T}_0 values. However, if $\mathcal{T}_0 \ll \sigma_e/\pi$ is very short, this may result in two-color seeding.

VII. ACKNOWLEDGMENTS

We gratefully acknowledge useful discussions with Zhi-Rong Huang, Gregory Penn, L.H. Yu, and Sven Reiche.

ZhiRong Huang and Juhao Wu are acknowledged for providing LCLS FEL parameters. Work at Brookhaven National Laboratory was supported by the U.S. Department of Energy, Office of Science, Office of Basic Energy Sciences, under Contract No. DE-AC02-98CH1-886. Work at Argonne National Laboratory was supported by the U.S. Department of Energy, Office of Science, under Contract No. DE-AC02-06CH11357.

-
- [1] G. Geloni, V. Kocharyan, and E. Saldin, *Journal of Modern Optics* **58**, 1391 (2011).
- [2] J. Amann, W. Berg, V. Blank, F.-J. Decker, Y. Ding, P. Emma, Y. Feng, J. Frisch, D. Fritz, J. Hastings, et al., *Nature Photonics* **6** (2012).
- [3] Yu. Shvyd'ko and R. Lindberg, *Phys. Rev. ST Accel. Beams* **15**, 100702 (2012).
- [4] E. Allaria, R. Appio, L. Badano, W. Barletta, S. Bassanese, S. Biedron, A. Borga, E. Busetto, D. Castronovo, P. Cinquegrana, et al., *Nature Photonics* **6**, 699704 (2012).
- [5] Y. Jiao, J. Wu, Y. Cai, A. Chao, W. M. Fawley, J. Frisch, Z. Huang, H.-D. Nuhn, C. Pellegrini, and S. Reiche, *Phys. Rev. ST Accel. Beams* **15**, 050704 (2012).
- [6] *Nuclear Instruments and Methods in Physics Research* **193**, 415 (1982), ISSN 0167-5087.
- [7] R. Bonifacio, C. Pellegrini, and L. Narducci, *Opt. Commun.* **50**, 373378 (1984).
- [8] K.-J. Kim, *Phys. Rev. Lett.* **57**, 1871 (1986).
- [9] E. L. Saldin, E. A. Schneidmiller, and M. V. Yurkov, *The Physics of Free Electron Lasers*, Advanced Texts in Physics (Springer, Berlin Heidelberg, 2000).
- [10] Z. Huang and K.-J. Kim, *Phys. Rev. ST Accel. Beams* **10**, 034801 (2007).
- [11] J. Feldhaus, E. Saldin, J. Schneider, E. Schneidmiller, and M. Yurkov, *Opt. Commun.* **140**, 341 (1997).
- [12] E. L. Saldin, E. A. Schneidmiller, Yu. V. Shvyd'ko, and M. V. Yurkov, *Nucl. Instrum. Methods Phys. Res. A* **475**, 357 (2001).
- [13] Y. Ding, Z. Huang, and R. D. Ruth, *Phys. Rev. ST Accel. Beams* **13**, 060703 (2010).
- [14] S. Reiche, *Nucl. Instrum. Methods Phys. Res. A* **429**, 243 (1999).
- [15] R. R. Lindberg and Yu. V. Shvyd'ko, *Phys. Rev. ST Accel. Beams* **15**, 050706 (2012).
- [16] Yu. Shvyd'ko, *X-Ray Optics – High-Energy-Resolution Applications*, vol. 98 of *Optical Sciences* (Springer, Berlin Heidelberg New York, 2004).
- [17] E. Saldin, E. Schneidmiller, and M. Yurkov, *Opt. Commun.* **148**, 383403 (1998).
- [18] P. Emma, R. Akre, J. Arthur, R. Bionta, C. Bostedt, J. Bozek, A. Brachmann, P. Bucksbaum, R. Coffee, F.-J. Decker, et al., *Nature Photonics* **4**, 641 (2010).
- [19] M. Cornacchia, S. Di Mitri, and G. Penco, *Phys. Rev. ST Accel. Beams* **9**, 120701 (2006).
- [20] K. L. F. Bane and G. Stupakov, *Nucl. Instrum. Methods Phys. Res. A* **690**, 106 (2012).
- [21] R. R. Lindberg, K.-J. Kim, Yu. Shvyd'ko, and W. M. Fawley, *Phys. Rev. ST Accel. Beams* **14**, 0110701 (2011).
- [22] M. Altarelli, R. Brinkmann, M. Chergui, W. Decking, B. Dobson, S. Dusterer, G. Grübel, W. Graeff, H. Graafsma, J. Hajdu, et al., *XFEL: The European X-Ray Free-Electron Laser : Technical design report* (DESY, Hamburg, 2006).
- [23] E. Burkel, *Rep. Prog. Phys.* **63**, 171 (2000).
- [24] M. Krisch and F. Sette, *Light Scattering in Solids IX* (Springer, Berlin, 2007), vol. 108 of *Topics in Applied Physics*, chap. Inelastic X-Ray Scattering from Phonons, pp. 317–370.
- [25] L. J. P. Ament, M. van Veenendaal, T. P. Devereaux, J. P. Hill, and J. van den Brink, *Rev. Mod. Phys.* **83**, 705 (2011).
- [26] Yu. Shvyd'ko, *Proc. SPIE, Advances in X-Ray/EUV Optics and Components VII* **8502**, 85020J (2012).
- [27] Yu. Shvyd'ko, S. Stoupin, K. Mundboth, and J. Kim, *Phys. Rev. A* **87**, 043835 (2013).
- [28] E. Gerdau and H. de Waard, eds., *Nuclear Resonant Scattering of Synchrotron Radiation* (Baltzer, 1999/2000), special issues of the *Hyperfine Interact.*, Vol. 123-125.
- [29] R. Röhlberger, *Nuclear Condensed Matter Physics with Synchrotron Radiation. Basic Principles, Methodology and Applications*, vol. 208 of *Springer Tracts in Modern Physics* (Springer Verlag, Berlin-Heidelberg, 2004).